5-2018

Modeling and analysis of variable reactive power limits of a Doubly Fed Induction Generator (DFIG) used in variable speed wind turbines

Jonathan Devadason
University of Tennessee, jdevadas@vols.utk.edu

To the Graduate Council:

I am submitting herewith a thesis written by Jonathan Devadason entitled "Modeling and analysis of variable reactive power limits of a Doubly Fed Induction Generator (DFIG) used in variable speed wind turbines." I have examined the final electronic copy of this thesis for form and content and recommend that it be accepted in partial fulfillment of the requirements for the degree of Master of Science, with a major in Electrical Engineering.

Hector A. Pulgar, Major Professor

We have read this thesis and recommend its acceptance:

Seddik M. Djouadi, Kai Sun

Accepted for the Council:
Dixie L. Thompson

Vice Provost and Dean of the Graduate School

(Original signatures are on file with official student records.)

Modeling and analysis of variable reactive power limits of a Doubly Fed Induction Generator (DFIG) used in variable speed wind turbines

A Thesis Presented for the

Master of Science

Degree

The University of Tennessee, Knoxville

Jonathan Devadason

May 2018

Dedicated to my dear parents Dr. Reenie Devadason and Mr.Joseph Devadason, my little brother Moses Devadason and my grandmother, Late.Mrs.Jessie Muthumani...

Acknowledgments

I express my deepest thanks to my Higher Power without Whom this task would have been impossible.

I would like to thank Dr. Hector Pulgar - Painemal for his excellent guidance in this work. I would also like to thank Dr. Kai Sun, Dr. Seddik Djouadi and Dr. Fangxing Li for all their encouragement and support in this endeavor.

I am greatly indebted to my parents Dr.Reenie Devadason and Mr. Joseph Devadason for their wonderful support and encouragement to follow my passion. I also want to mention my friends in UT and my ministers Ben Winder, Scott Claybrook and Susan Tatum for helping me stay motivated through the entire duration of this thesis.

Finally, I would like to express my deepest appreciation to the staff of Ebenezer counseling services and Blount Memorial hospital for the care they provided during the most crucial part of this research.

Abstract

In this thesis, the mathematical modeling of variable reactive power limits for a Doubly Fed Induction Generator (DFIG) based on its capability curves is presented. Reactive power limits have been adjusted dynamically based on the capability curves when the system was subjected to a disturbance. This ensures that the operation of the DFIG is always within safe limits and utilizes the available capability of the DFIG to improve the performance of the system.

The small signal stability of the system is studied by considering the load as a variable parameter. The differential-algebraic model of the DFIG, synchronous generators and their associated controllers and the power system network is linearized and bifurcation analysis considering the load as the bifurcation parameter has been performed. The PV curves, the stator and rotor current magnitudes, and the eigenvalue trajectories are plotted as the load is varied. Time domain simulations are performed to observe the change in stator and rotor currents when the system is subjected to a load change and a change in the wind speed.

The system considered for testing is the IEEE 9 bus system which is modified to include a wind farm consisting of 5 wind turbines. The variable reactive power limits are implemented in the reactive power controller of the DFIG and the performance of the system is compared to that of the system with fixed limits in the reactive power controller. From the bifurcation analysis, it was observed that the stator and rotor currents were at the maximum limits when the lower and upper limits of the controller were reached. Also, the Hopf bifurcation was found to occur at a lower load level compared to the system with fixed reactive power limits. From the time domain simulations, it was observed that the stator and rotor currents did not exceed the maximum limits in the system with variable reactive power limits when the system was subjected to a change in the load and a change in the wind speed. Hence,

the problem of over/under estimating the reactive power capability of the DFIG based wind farm was avoided.

Table of Contents

List of Tables

List of Figures

Chapter 1

Introduction

Nowadays, the world is moving towards clean forms of energy. This is mainly due to the global warming issues due to the emission of CO_2 into the atmosphere and one of the main contributors to this are the conventional power plants.This would lead to other problems like acid rain [1] and greenhouse effect [2]. Also,there is a depletion of fossil fuels in the earth [3]. All these reasons have led to the increase in the deployment of renewable energy resources [4]. Wind is one of the cleanest forms of energy.Also, the cost of production of energy from wind has come down in the recent years [5].

1.1 Types of wind turbines

Wind turbines are classified into three types - Fixed speed (Type A), semi variable speed (Type B) and variable speed wind turbines (Type C) [6],[7], [8]. The fixed speed wind turbines are usually based on Squirrel Cage Induction Generators (SCIGs) which provide output only through the stator winding. It requires a grid connected SCIG coupled to the wind turbine through a gear box. Because of the coupling to the grid, the speed varies over a very small range (usually around 1%), hence commonly known as fixed speed system. At speeds other than the rated wind speed, fluctuations in the wind speed leads to pulsations in the torque (power) which leads to grid voltage fluctuations and strain on the gear box. Also, these generators always consume reactive power from the grid and hence, capacitors need to be installed to compensate for this.

In semi - variable speed operation, some of the generator shaft power is dissipated in the rotor, the pulsations in the power is reduced under fluctuating wind conditions. The variation of the rotor resistance with the slip is maintained constant which keeps the rotor current and the airgap power constant.

Variable speed wind turbines are more advantageous when compared to the other two technologies. This makes use of a wound rotor induction generator. Bidirectional power flow through the rotor circuit is achieved by utilizing an ac-dc-ac converter between the slip ring terminals and the grid. The converter can be fully or partially rated. Full rated converters are more expensive than partially rated ones and hence, sparingly used. Here, we limit ourselves to the study of a wind turbine with partially rated converters as this is less expensive. The rating of the converter is usually 25 - 30% of the rating of the machine. The arrangement consists of an induction generator with a back to back converter connecting the grid and the rotor circuit. This is called 'Doubly Fed Induction Generator (DFIG)'.

1.2 Wind turbines participation in frequency and voltage regulation

Modern grid codes demand wind power plants to participate in frequency regulation [9], [10]. This leads to increased real power generation for short amounts of time requiring regulation of active power.

It is advantageous to maintain the voltage at a remote bus at a reference value using a supervisory control mechanism which generates the reactive power needed to regulate the voltage at the remote bus [11]. But with the load in the system increasing and the wind turbines also participating in frequency regulation, the availability of reactive power obtained from the DFIG based wind turbines is limited. In the existing literature, the DFIG is implemented with either limits on the individual PI controllers controlling the reactive power limits, d component of the rotor current and the d component of the rotor voltage or just having a supervisory control mechanism with no limits implemented in the DFIG.

In this thesis, two different models of reactive power limits based on the capability curve equations are presented.

1.3 State of the art

The voltage at a bus in a power system can be regulated by controlling the rotor and the grid side converters [12]. In order to do this, there should be sufficient amount of reactive power capability from the wind farm. The rotor angle stability of the power system can be improved by controlling the terminal voltage of the DFIG [13]. Additional reactive power is available from the DFIG based wind farm when it is operated based on the capability curves [14].It is possible to control the DFIG based wind turbine so it can provide voltage regulation, frequency regulation and oscillation damping by controlling the magnitude and angle of the rotor flux [15]. The reactive power capability of the wind farm depends on the operating slip and the real power output of the wind farms which in turn depends on the wind speed. Hence, there is a possibility of over/under estimating the reactive power capability of the wind farms which may lead to unsafe operation due to the violation of operating limits.

The availability of additional reactive power from a DFIG based wind farm by utilizing the capability curve of the machine is described in reference[16]. Here, only the underutilization of reactive power capability of wind farms by operating at a fixed power factor has been discussed. The effects of wind speed variations and the impact of the availability of additional reactive power on the small signal stability of the system has not been analyzed. The control of DFIG based wind turbine so as to provide frequency regulation, oscillation damping and voltage control is described in reference [15]. A Flux Magnitude and Angle Controller (FMAC) is used to provide the control mechanism by adjusting the rotor flux vector magnitude and angle. The effect on the reactive power output of the DFIG is not discussed here.

1.4 Literature review

Reference [17] describes the capability curves of the DFIG and a main observation made is that under normal operating values of slip, the stator current plays a limiting role in the absorption of reactive power and the rotor current limits the production of reactive power.

In reference [18], the capability curves of the DFIG have been obtained considering the limitations in converter currents, junction temperature and saturation effects. But in this thesis, the non linearities with respect to saturation and temperature effects have not been considered for the sake of simplicity.

The steady state model of the DFIG, the coupling effects between the q-component of the rotor current and the active power as well as the d-component of the rotor current and the reactive power and the capability curves of the DFIG have been described in reference [19]. The steady state model described in this article is adopted for the study conducted in this thesis.

The requirements which have to be met when wind farms are connected to the grid with respect to real and reactive power control, voltage control and frequency control and supporting grid voltage under the occurrence of faults have been discussed in references [20] and [9]. The participation of DFIG based wind farms in regulating real power and frequency will affect the reactive power capability available for the controlling the voltage.

The mathematical modeling of induction machines based on the reference frame theory is explained in reference [21] which has been applied in this study to derive the mathematical model of the DFIG.

The mathematical model of DFIG based wind farms and the control schemes has been presented in reference [22]. The data of the 3.6 MVA wind farm in this article has been used for the DFIG based wind turbines in this thesis. The mathematical modeling of a DFIG, pitch angle controller, terminal voltage controller and a speed controller has been presented in reference [23] based on which the DFIG was initialized for bifurcation analysis and time domain simulations in this study.

The ability of the DFIG to provide frequency regulation through inertial response by utilizing additional control loops is discussed in references [24] and [25].

The application of bifurcation theory to power systems has been discussed in reference [26]. The different kinds of bifurcations which might occur in a power system and the issues related to loading are summarized in reference [27]. The load at a bus is considered as a bifurcation parameter which has been adapted in this thesis as well.

The utilization of FACTS devices to eliminate bifurcations in the power system is described in reference [28]. The comparison of the performance of different FACTS devices in eliminating bifurcations is presented in reference [29]. With the utilization of the capability curves in the DFIG, the reactive power availability will be reduced during periods of high active power production and under disturbances when the DFIG participates in frequency regulation. A co-ordinated control between the DFIG and the FACTS devices can be explored as an extension of the work done in this thesis.

1.5 Organization of the thesis

This thesis is organized as follows: The mathematical model of the wind turbine controllers are presented in chapter 2. Chapter 3 presents the mathematical modeling of the reactive power limits of the DFIG, chapter 4 describes the test system considered and the results and analysis of the same. The conclusion is presented in chapter 5.

Chapter 2

Mathematical modeling of DFIG controllers

The mathematical model used in this thesis for the DFIG based wind farm is based on reference [11].The stator and rotor transients are assumed to be very fast and hence, they are neglected. The detailed mathematical model of the DFIG can be found in reference [30].

The wind turbine shaft is modeled by a single mass. The mathematical models of the wind turbine and the shaft sections can be found in reference [11]. In this study, stator flux orientation has been assumed for the DFIG which allows independent control real and reactive power. There are different controllers in the DFIG to control voltage, active power, reactive power and inertial and pitch controllers depending on whether the DFIG participates in frequency regulation or not. The mathematical models of the different controllers have been derived in the following sections.

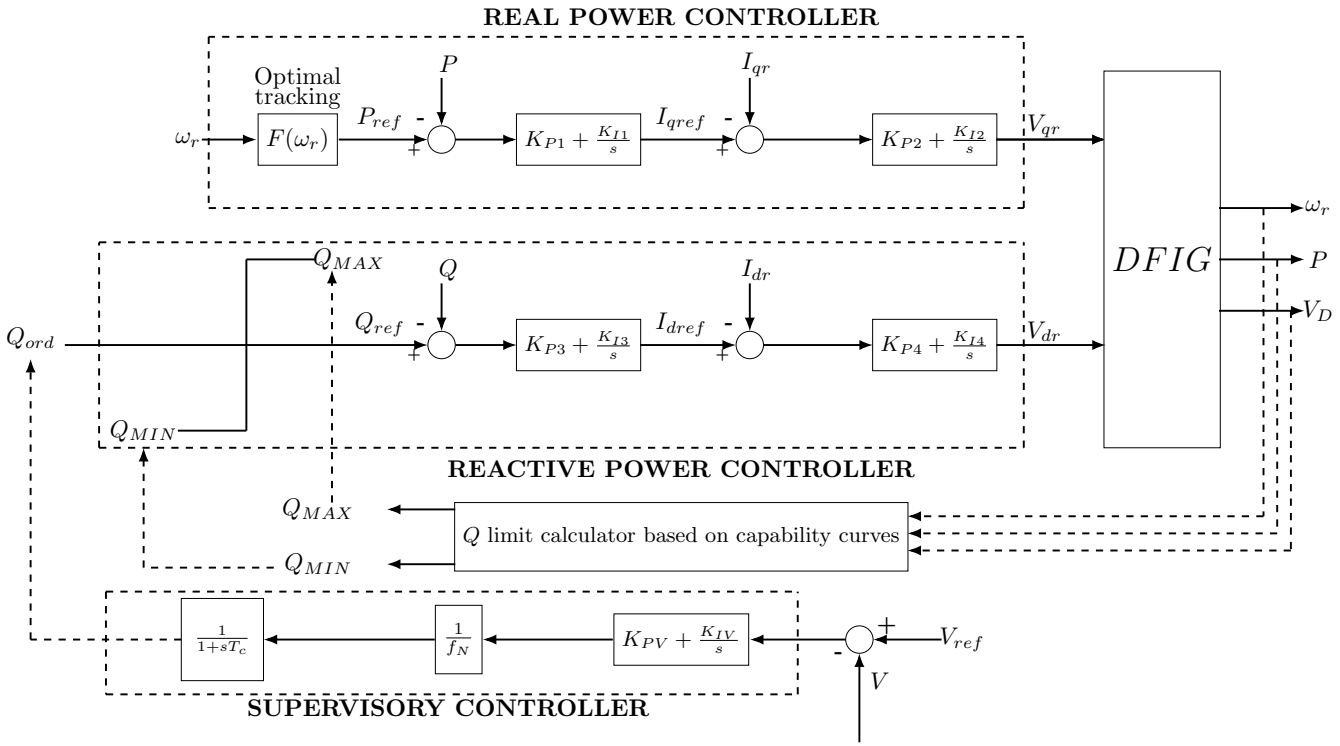

Figure 2.1: Control system of the DFIG

2.1 Control of active and reactive power

The block diagram for the active and reactive power control and supervisory control of the DFIG is shown in figure 2.1.

2.1.1 Active power control

The active power is regulated at the reference value P_{ref} which is obtained from the Maximum Power Point Tracking curve ($MPPT$) which has been approximated by the equation

$$P_{ref} = C\omega_r^3 \tag{2.1}$$

where C is a parameter which is tuned [31]. The resulting error in the active power is processed by a PI controller which generates the reference signal corresponding to the q-component of the rotor current (I_{qref}). The error in the q-component of the rotor current is processed by a second PI controller which generates the signal V_{qr} which is the q-component of the rotor voltage which is injected into the rotor to control active power. The state and algebraic equations corresponding to the active power controller are derived as shown below:

$$\dot{x_1} = K_{I1}(P_{ref} - P) \tag{2.2}$$

$$\dot{x_2} = K_{I2}(I_{qref} - I_{qr}) \tag{2.3}$$

$$I_{qref} = K_{P1}(P_{ref} - P) + x_2 \tag{2.4}$$

$$V_{qr} = K_{P2}(I_{qref} - I_{qr}) \tag{2.5}$$

2.1.2 Reactive power control

The reactive power reference is obtained from the supervisory voltage controller. The error in the reactive power is processed by a PI controller which generates the d-component of the rotor current (I_{dref}). The difference in I_{dref} and the d-component of the rotor current (I_{dr}) is processed by a second PI controller which dictates the d-component of the voltage (V_{dr})

to be injected into the rotor to control the reactive power. The equations pertaining to the reactive power controller are given below:

$$\dot{x_3} = K_{I3}(Q_{ref} - Q) \tag{2.6}$$

$$\dot{x_4} = K_{I4}(I_{dref} - I_{dr}) \tag{2.7}$$

$$I_{dref} = K_{P1}(Q_{ref} - Q) + x_3 \tag{2.8}$$

$$V_{dr} = K_{P2}(I_{dref} - I_{dr}) + x_4 \tag{2.9}$$

2.1.3 Supervisory control

The block diagram of the supervisory control is also shown in figure 2.1. It consists of a PI controller, the input of which is the voltage error $(V_{ref} - V)$.The output of this controller is the reactive power which is needed to regulate the voltage of the remote bus at V_{ref}. The constant f_N is fraction which indicates the total number of wind turbines under operation. The reactive power reference is scaled by the factor $\frac{1}{f_N}$ which is the reactive power reference which has to be supplied to all the wind turbines. A first order block with time constant T_c is considered to take into account, the communication delay between the supervisory controller and the individual wind turbines [11].

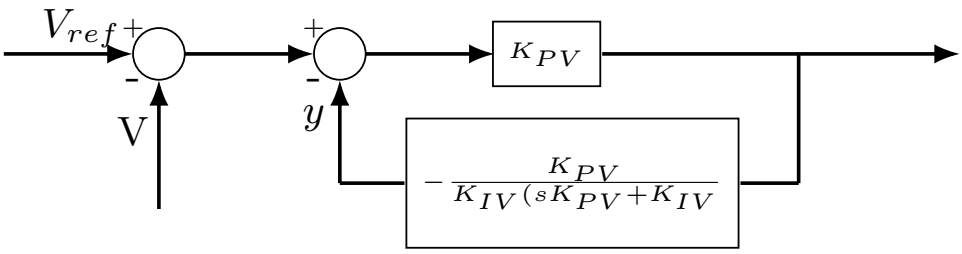

Figure 2.2: Modified representation of the voltage controller

The mathematical model of the PI controller controlling the voltage is represented as shown in figure 2.2 so that the limits can be applied on the algebraic equation which represents the reactive power reference [11]. This is done just for ease of computation. The equations representing this are

$$H(s) = K_{PV} + \frac{K_{IV}}{s} \tag{2.10}$$

Equation (2.10) can be expressed in the form

$$H(s) = \frac{H_1(s)}{1 + H_1(s)H_2(s)} \tag{2.11}$$

where

$$H_1(s) = K_{PV} \tag{2.12}$$

$$H_2(s) = \frac{-K_{IV}}{K_{PV}(sK_{PV} + K_{IV})} \tag{2.13}$$

The differential equations corresponding to the supervisory control are given below:

$$\dot{y} = -\frac{K_{IV}}{K_{PV}}y - \frac{K_{IV}}{K_{PV}^2} \tag{2.14}$$

$$\dot{Q_{ord}} = \frac{1}{T_c f_N}Q_c - \frac{1}{T_c}Q_{ord} \tag{2.15}$$

where

$$Q_c = K_{PV}(V_{ref} - V - y) \tag{2.16}$$

2.2 Participation of a DFIG in frequency regulation

In this section, two control schemes of the DFIG to provide frequency regulation in the event of a disturbance in the power system is presented [31].

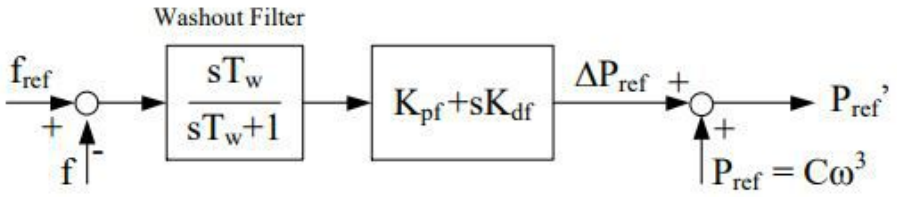

Figure 2.3: Control scheme to provide frequency regulation through inertial response

2.2.1 Inertial response of DFIG wind turbines

The block diagram describing the control scheme to provide inertial response is shown in figure 2.3. In this scheme, the kinetic energy stored in the wind turbine mass is used to provide/absorb power when there is an under/over frequency condition. The function of the washout filter is to ensure that the control acts only during the first moment of deviation.

2.2.2 Frequency regulation through pitch control of wind turbines

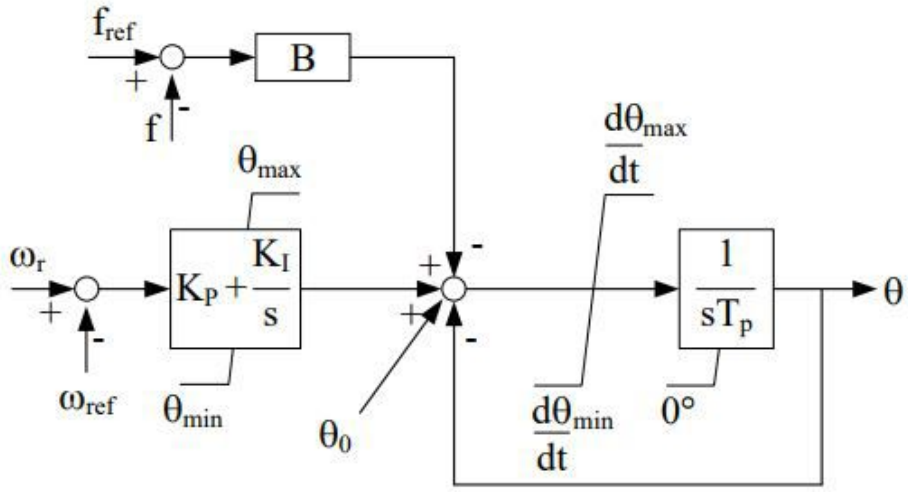

Figure 2.4: Control scheme to provide frequency regulation through pitch control

Figure 2.4 shows the control scheme adopted to provide frequency control by pitching the blades of the wind turbine. The wind turbine is operated at a lower power at every point to reserve an amount of margin which allows for controlling frequency by injecting/absorbing power in the event of a disturbance. The disadvantage in this scheme is that the overall

power which is produced for a given wind speed is reduced which results in reduced revenue for the owner of the wind farm.

Chapter 3

Mathematical modeling of variable reactive power limits of the DFIG

In this chapter, the importance of capability curves and the mathematical modeling of reactive power limits of the DFIG are presented. The main reason to implement variable reactive power limits in the DFIG is because the reactive power depends on the real power and slip of the machine. Since the operation of the wind turbine is slow compared to the duration of the stator and rotor transients of the DFIG, the use of the capability curves to compute the reactive power limits is justified.

3.1 Capability curves

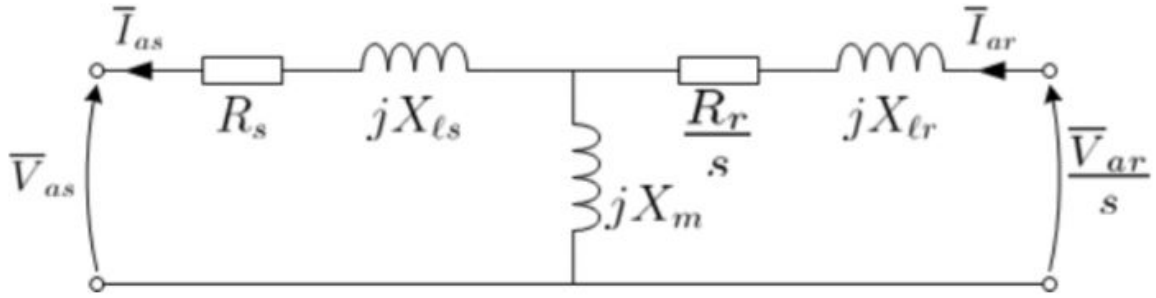

Figure 3.1: Equivalent circuit of a DFIG

The equivalent circuit of the DFIG which is considered in this study is shown in figure 3.1. The two port network matrices for the circuit can be obtained as

$$\begin{bmatrix} \overline{V}_{as} \\ \overline{I}_{as} \end{bmatrix} = \underbrace{\begin{bmatrix} -(R_s + jX_s) & jX_m \\ -jX_m & \frac{R_r}{s} + jX_r \end{bmatrix}}_{\text{Z}} \begin{bmatrix} \overline{I}_{as} \\ \overline{I}_{ar} \end{bmatrix} \tag{3.1}$$

$$\begin{bmatrix} \overline{I}_{as} \\ \overline{I}_{ar} \end{bmatrix} = Y \begin{bmatrix} \overline{V}_{as} \\ \frac{\overline{V}_{ar}}{s} \end{bmatrix} \tag{3.2}$$

where

$$Y = Z^{-1} \tag{3.3}$$

$$\begin{bmatrix} \overline{I}_{as} \\ \frac{\overline{V}_{ar}}{s} \end{bmatrix} = \underbrace{\begin{bmatrix} \frac{-1}{R_s+jX_s} & \frac{jXm}{R_s+jX_s} \\ \frac{jX_m}{R_s+jX_s} & \frac{R_r}{s} + jX_r + \frac{{X_m}^2}{R_s+jX_s} \end{bmatrix}}_{\text{G}} \begin{bmatrix} \overline{V}_{as} \\ \overline{I}_{ar} \end{bmatrix} \tag{3.4}$$

$$\begin{bmatrix} \frac{\overline{V}_{ar}}{s} \\ \overline{I}_{ar} \end{bmatrix} = \underbrace{\begin{bmatrix} \frac{\frac{R_r}{s}+jX_r}{jX_m} & \frac{(\frac{R_r}{s}+jX_r)(R_s+jX_s)+{X_m}^2}{jX_m} \\ \frac{1}{jX_m} & \frac{R_s+jX_s}{jX_m} \end{bmatrix}}_{\text{B}} \begin{bmatrix} \overline{V}_{as} \\ \overline{I}_{ar} \end{bmatrix} \tag{3.5}$$

The DFIG has three operating limits - Rotor current limit,Stator current limit and Rotor voltage limit. The capability curves of a DFIG for two different slips of operation are represented in figures 3.2 and 3.3. In figure 3.2, it can be observed that the rotor current limits the operation when reactive power is supplied to the grid and the stator current limits the operation when reactive power is drawn from the grid. But when the slip increases, the rotor voltage curve moves downward and limits the operation of the DFIG.

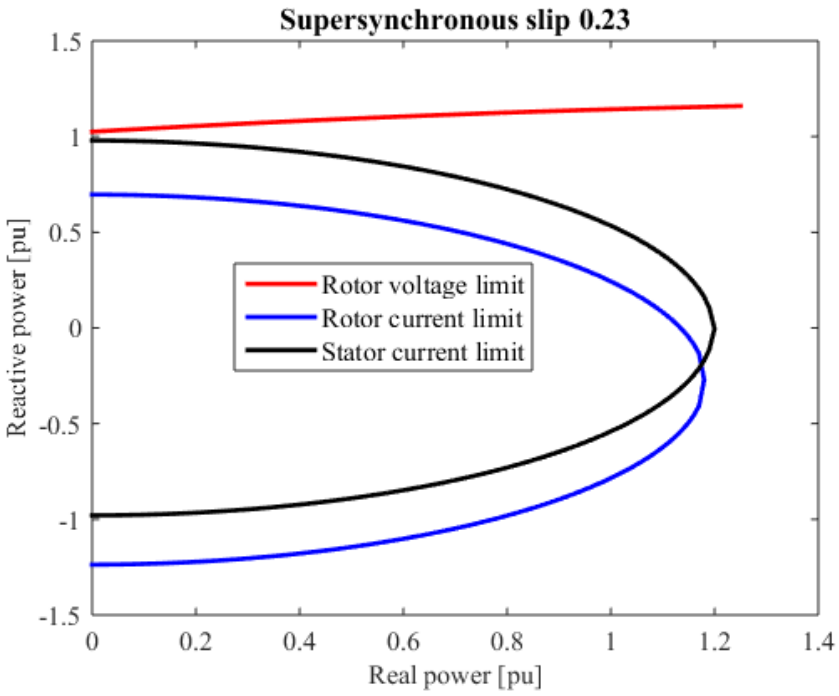

Figure 3.2: Capability curves for a supersynchronous slip of 0.23

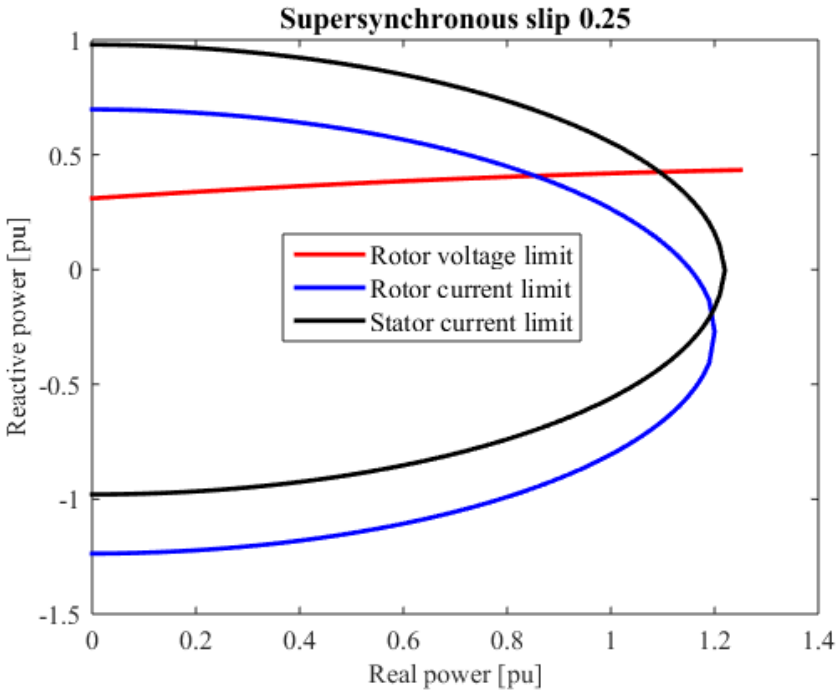

Figure 3.3: Capability curves for a supersynchronous slip of 0.25

3.2 Mathematical modeling of reactive power limits

The reactive power limits related to the rotor voltage have been derived in the following section. The losses in the DFIG are not neglected which makes the equation a bit complex. The modeling of the limits neglecting the losses will be shown in section 3.2.2.

3.2.1 Modeling of rotor voltage limits of the DFIG considering the losses

The elements of the admittance matrix Y (equations 3.2 and 3.3) can be represented as:

$$Y = \begin{bmatrix} G_{11} + jB_{11} & G_{12} + jB_{12} \\ G_{21} + jB_{21} & G_{22} + jB_{22} \end{bmatrix} \tag{3.6}$$

The complex power delivered by the stator is given by the equation

$$S_s = \overline{V}_{as} \overline{I}_{as}{}^{*} \tag{3.7}$$

where

$$\overline{V}_{as} = V_s \tag{3.8}$$

$$\overline{V}_{ar} = V_r e^{j\beta} \tag{3.9}$$

The complex power at the stator S_s can also be expressed as

$$S_s = P_s + jQ_s \tag{3.10}$$

where P_s and Q_s is the real and reactive power delivered by the stator. Expressing $\overline{V}_{as}$ and $\overline{I}_{as}$ in terms of the elements of the Y matrix, P_s and Q_s can be written as

$$P_s = G_{11}{V_s}^2 + \frac{V_s V_r}{s}(G_{12}\cos\beta - B_{12}\sin\beta) \tag{3.11}$$

$$Q_s = -B_{11}{V_s}^2 - \frac{V_s V_r}{s}(G_{12}\sin\beta + B_{12}\cos\beta) \tag{3.12}$$

The complex power delivered to the rotor is given by the equation

$$S_r = \overline{V}_{ar}\overline{I}_{ar}{}^{*} \tag{3.13}$$

If P_r and Q_r represents the real and reactive power delivered to the rotor, the complex power is also expressed as

$$S_r = P_r + jQ_r \tag{3.14}$$

Similarly, expressing $\overline{V}_{ar}$ and $\overline{I}_{ar}$ in terms of the elements of the Y matrix, P_r and Q_r can be written as

$$P_r = \frac{V_r{}^2}{s}G_{22} + V_sV_r(G_{21}\cos\beta + B_{21}\sin\beta) \tag{3.15}$$

$$Q_r = \frac{-V_r{}^2}{s}B_{22} + V_sV_r(G_{21}\sin\beta - B_{21}\cos\beta) \tag{3.16}$$

The net real power generated is given by

$$P_G = P_s - P_r \tag{3.17}$$

The reactive power consumed by the rotor is supplied by the rotor side converter and hence, the net reactive power generated is represented as

$$Q_G = Q_s \tag{3.18}$$

Substituting equations 3.11 and 3.15 in equation 3.17, P_G can be written as

$$P_G = k_1 + A_1\cos\beta + B_1\sin\beta \tag{3.19}$$

where

$k_1 = V_s{}^2G_{11} - \frac{V_r{}^2}{s}G_{22}$

$A_1 = V_sV_r(\frac{G_{12}}{s} - G_{21})$

$B_1 = -V_s V_r(\frac{B_{12}}{s} + B_{21})$

Now, equation 3.19 is rewritten as

$$P_G - k_1 = R_1 \cos(\beta - \alpha) \tag{3.20}$$

where

$R_1 = \sqrt{{A_1}^2 + {B_1}^2}$

$\tan\alpha = B_1/A_1$

Let

$$(P_G - k_1)/R_1 = \cos\gamma \tag{3.21}$$

Hence, equation 3.21 becomes

$$\cos(\beta - \alpha) = \cos\gamma \tag{3.22}$$

The solution for β from equation 3.22 is given by

$$\beta = \alpha \pm \gamma \tag{3.23}$$

Let

$$\begin{cases} \beta_1 = \alpha + \gamma \\ \beta_2 = \alpha - \gamma \end{cases} \tag{3.24}$$

The equation for the generated reactive power is expressed as

$$Q_G = -B_{11}{V_s}^2 - \frac{V_s V_r}{s}(G_{12}\sin\beta + B_{12}\cos\beta) \tag{3.25}$$

where Q_G can be calculated for β_1 and β_2 which are functions of the slip and the real power generated for that particular value of slip. Out of the two solutions for Q_G, the higher one

corresponds to the maximum value and the other value corresponds to the minimum value of reactive power that can be produced.

3.2.2 Reactive power limits neglecting losses in the DFIG circuit

When the resistances R_s and R_r are neglected in the rotor circuit, the equations are much simpler and are presented in this section. The impedance matrix Z is now modified as

$$Z = \begin{bmatrix} -jX_s & jX_m \\ -jX_m & jX_r \end{bmatrix} \tag{3.26}$$

Taking the inverse of equation 3.27, the admittance matrix Y has been derived as

$$Y = \frac{1}{\Delta Z} \begin{bmatrix} jX_r & -jX_m \\ jX_m & -jX_s \end{bmatrix} \tag{3.27}$$

where

$$\Delta Z = X_s X_r - X_m^2 \tag{3.28}$$

Following a similar procedure described in the section 3.2, the real and reactive power delivered by the stator (P_s and Q_s respectively) are given by the following equations:

$$P_s = \frac{X_m}{s\Delta Z} V_s V_r \sin\beta \tag{3.29}$$

$$Q_s = \frac{X_m}{s\Delta Z} V_s V_r \cos\beta - \frac{X_r}{\Delta Z} V_s^2 \tag{3.30}$$

The real and reactive power absorbed by the rotor circuit (P_r and Q_r) are given by the equations

$$P_r = \frac{X_m}{\Delta Z} V_s V_r \sin\beta \tag{3.31}$$

$$Q_r = \frac{X_s}{\Delta Z}\frac{V_r^2}{s} - \frac{X_m}{\Delta Z} V_s V_r \cos\beta \tag{3.32}$$

The net real power generated by the DFIG is given by the equations

$$P_G = P_s - P_r \tag{3.33}$$

$$P_G = \frac{X_m}{\Delta Z} V_s V_r (\frac{1}{s} - 1) \sin\beta \tag{3.34}$$

The reactive power generated by the DFIG considering that the reactive power consumed by the rotor is supplied by the rotor side converter, hence the reactive power generated is given by the equations

$$Q_G = Q_s - Q_r \tag{3.35}$$

$$Q_G = \frac{X_m}{s\Delta Z} V_s V_r \cos\beta - \frac{X_r}{\Delta Z} V_s^2 \tag{3.36}$$

Squaring and adding equations 3.34 and 3.36 to eliminate β, the resulting equation is

$$Q_G^2 + 2Q_G K_1 + K_1^2 - \frac{K_2^2}{s^2} + (\frac{P_G}{1-s})^2 = 0 \tag{3.37}$$

where

$K_1 = \frac{X_m}{\Delta Z} V_s V_r$

$K_2 = \frac{X_r}{\Delta Z} V_s^2$

Solving the quadratic equation 3.37, the reactive power generated is obtained as

$$Q_G = -\frac{X_r}{\Delta Z} V_s^2 \pm \sqrt{(\frac{X_m}{s\Delta Z} V_s V_r)^2 - (\frac{P_G s}{1-s})^2} \tag{3.38}$$

The higher value among the two solutions in equation 3.38 is the maximum reactive power and the other value is the minimum amount of reactive power that can be generated for a given slip and real power.

The real and reactive power equations considering the rotor current limit and the stator current limit can be obtained using a similar procedure adapted in sections 3.2.1 and 3.2.2 and is presented in the Appendices A and B.

Chapter 4

Results and analysis

The reactive power limit models derived in chapter 3 are implemented in a 15 bus test system comprising of 5 wind turbines as shown in figure 4.1 and the results are analyzed. The mathematical model of the synchronous machine and its associated controllers can be found in reference [32]. The load is considered to be a bifurcation parameter. This is because, the system load plays an important role in the stability of the system. The effect of a step change in the load and a change in the wind speed on the stator and rotor currents has been studied using time domain simulations and the results are analyzed. The data of the system is taken from reference [11].

4.1 Linearization of the power system model

The differential and algebraic equations which describe the dynamics of the system are linearized around different operating points which are obtained by varying the load in a certain bus in the system. The general form of the equations which describe the reactive power limits is given as

$$Q_{limit} = f(V_D, s, P) \tag{4.1}$$

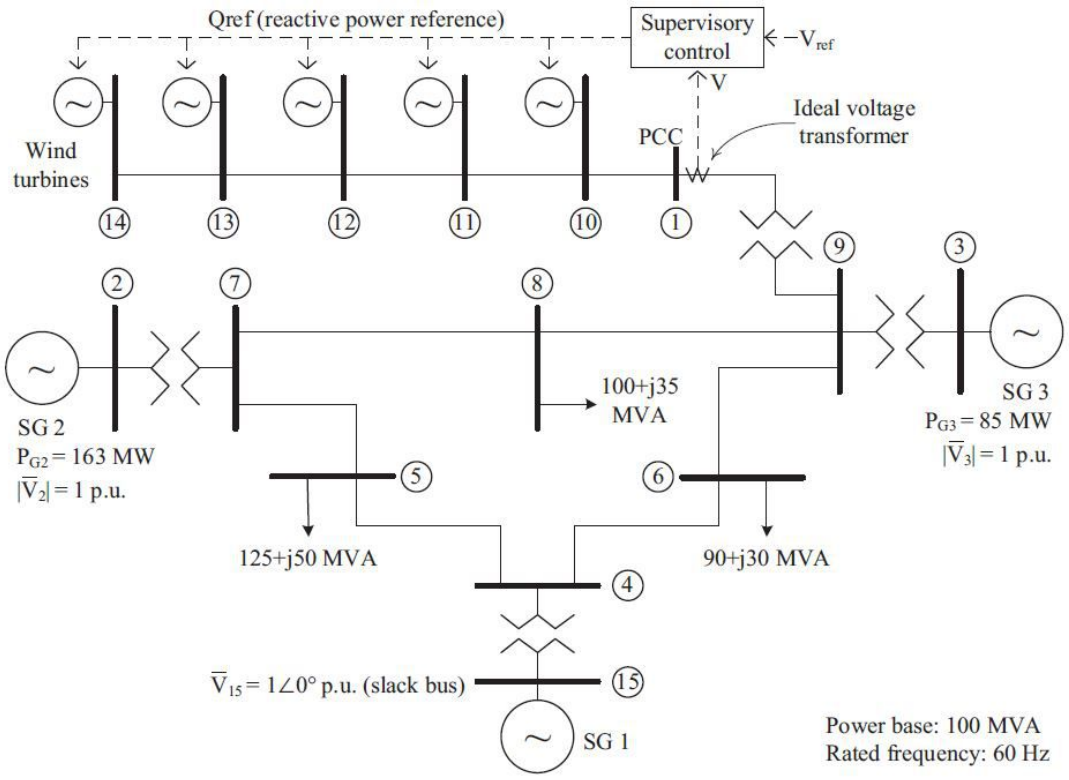

Figure 4.1: Test system considered for study

where V_D is the terminal voltage, s is the operating slip and P is the real power produced for the given operating slip. The linearized form of equation 4.1 is expressed as

$$\Delta Q_{limit} = K_1 \Delta V_D + K_2 \Delta w_r + K_3 \Delta P \tag{4.2}$$

where K_1,K_2 and K_3 are the constants which are calculated for a particular operating point.

The equations are cast in matrix form

$$\Delta \dot{X} = A\Delta X + B\Delta Y \tag{4.3}$$

$$0 = C\Delta X + D\Delta Y \tag{4.4}$$

Equation (4.4) can be rewritten as

$$\Delta Y = -D^{-1}C\Delta X \tag{4.5}$$

Substituting equation (4.5) in (4.3), the expression for $\Delta\dot{X}$ is obtained as

$$\Delta\dot{X} = (A - BD^{-1}C)\Delta X \tag{4.6}$$

$$A_{sys} = A - BD^{-1}C \tag{4.7}$$

where A_{sys} is the system matrix, the eigen values of which are calculated to study the stability of the system.

4.2 Simulation results

The test system consists of three load buses namely buses 5, 6 and 8. Let the system with no reactive power limits in the DFIG be denoted as system A and the system with reactive power limits implemented in the DFIG be denoted as system B. The bifurcation analysis of the system has been carried out considering the load at these buses as the bifurcation parameter and the variation of the voltage at the point of common coupling (V_{PCC}) is studied for the system with fixed reactive power limits and variable reactive power limits in the controller for reactive power. The time domain simulations are also performed in the system considering a step change in the load at bus 5. Also, a change in the wind speed is considered from 11 to 12 m/s. The plots of the stator and rotor currents with respect to time are described.

4.2.1 Analysis of PV curves

The load considered in this system is a constant power factor load. The active and the reactive power components of the load is increased in steps and the variation of the voltage V_{PCC} is plotted against the bifurcation parameter. In this case, it is the load at bus 6.

Figure 4.3 shows the variation of V_{PCC} with the active power load for the system with fixed reactive power limits. It is observed that between a load level of 10 MW to 82 MW, the voltage is above the reference value (1 p.u) because the controller is operating at the minimum reactive power limit. Between a load of 82 MW and 282 MW, the voltage is regulated at 1 p.u and when the load exceeds 282 MW, the voltage starts dropping from 1 p.u because the controller operates at the lower reactive power limit.

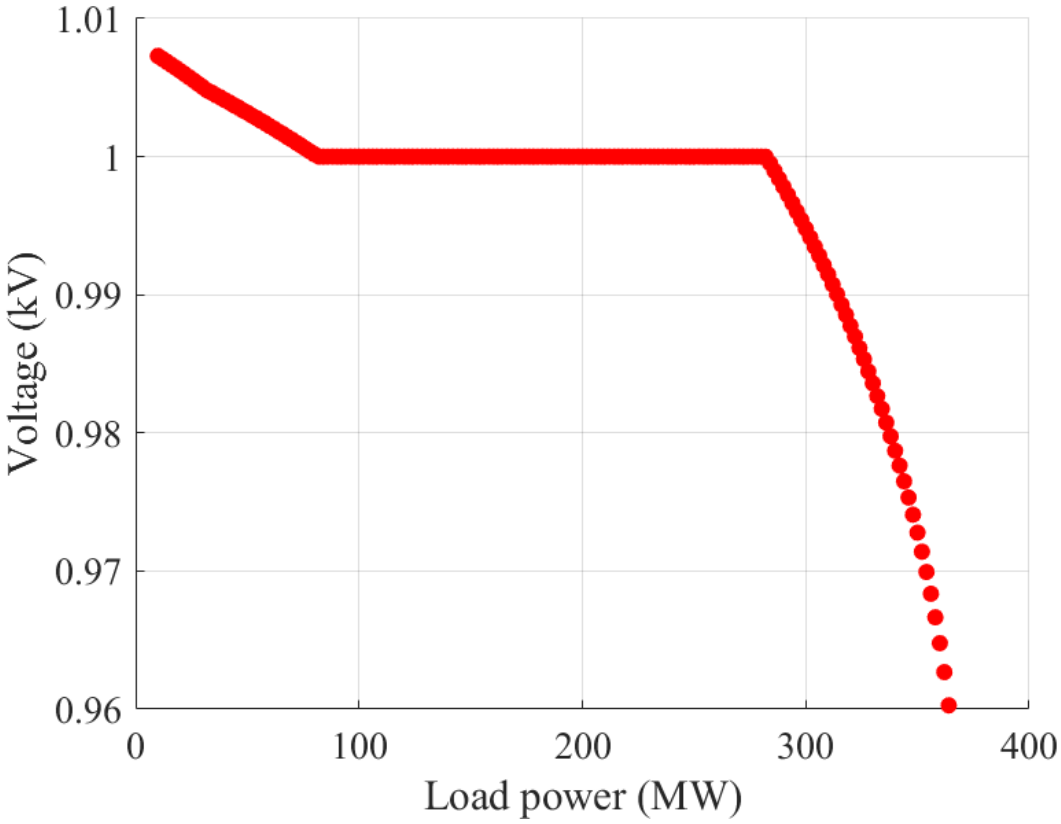

Figure 4.2: PV curve with fixed reactive power limits in the DFIG

In figure 4.3, the variation of the voltage at the PCC is plotted against the active power load at bus 6 when it is varied from 10 to 400 MW. The curve is of the same shape as that of figure 4.2 but the difference is that between a load of 10 MW and 82 MW, the lower limit of the supervisory control dictates the reactive power reference. The lower limit of the supervisory controller is imposed by the stator current limit. Between a load of 82 MW and 250 MW, the voltage was regulated at 1 p.u and when the load exceeds 250 MW, the voltage drops from 1 p.u because now, the reactive power limit is because of the rotor current limit. From figures 4.2 and 4.3, it is clear that the estimated reactive power available to regulate the voltage at the PCC was lower than what was actually available in the system.

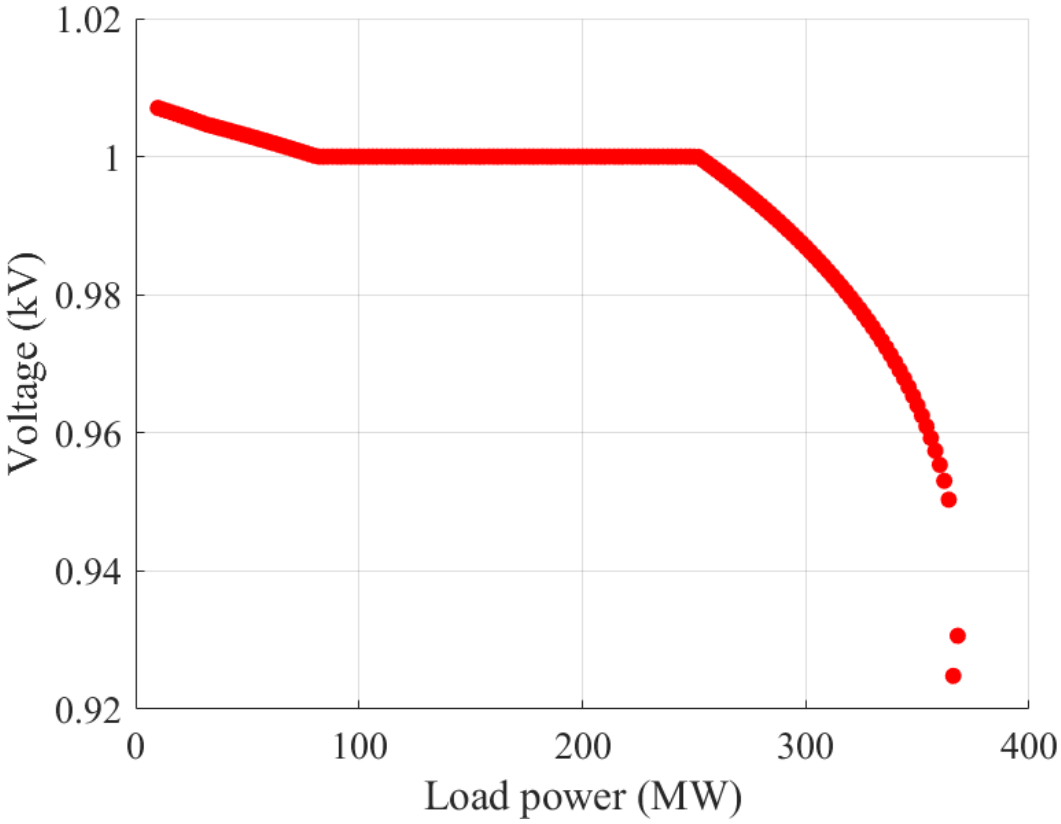

Figure 4.3: PV curve with variable reactive power limits in the DFIG

4.2.2 Variation of stator and rotor currents with load

In figure 4.4, the variation of the stator and rotor currents with the active power load is shown. From a loading level of 82 MW to 282 MW, the stator and rotor currents are within the allowable limits but when the load is increased past 282 MW, the stator and rotor currents surpass the maximum limits.

When figure 4.5 is observed, it can be observed that when the load is between 10 and 82, the stator current is at its maximum limit and between the load of 82 and 250, the rotor current is at the maximum limit. Between 250 and 364, the system operates in the region inside the capability curve and hence, the stator and rotor currents are well within the limits.

The load levels at which a Hopf bifurcation occurs for maintaining V_{PCC} at 0.98 p.u and 1 p.u by performing the bifurcation analysis in systems A and B considering the loads at buses 5, 6 and 8 as the bifurcation parameters are summarized in table .

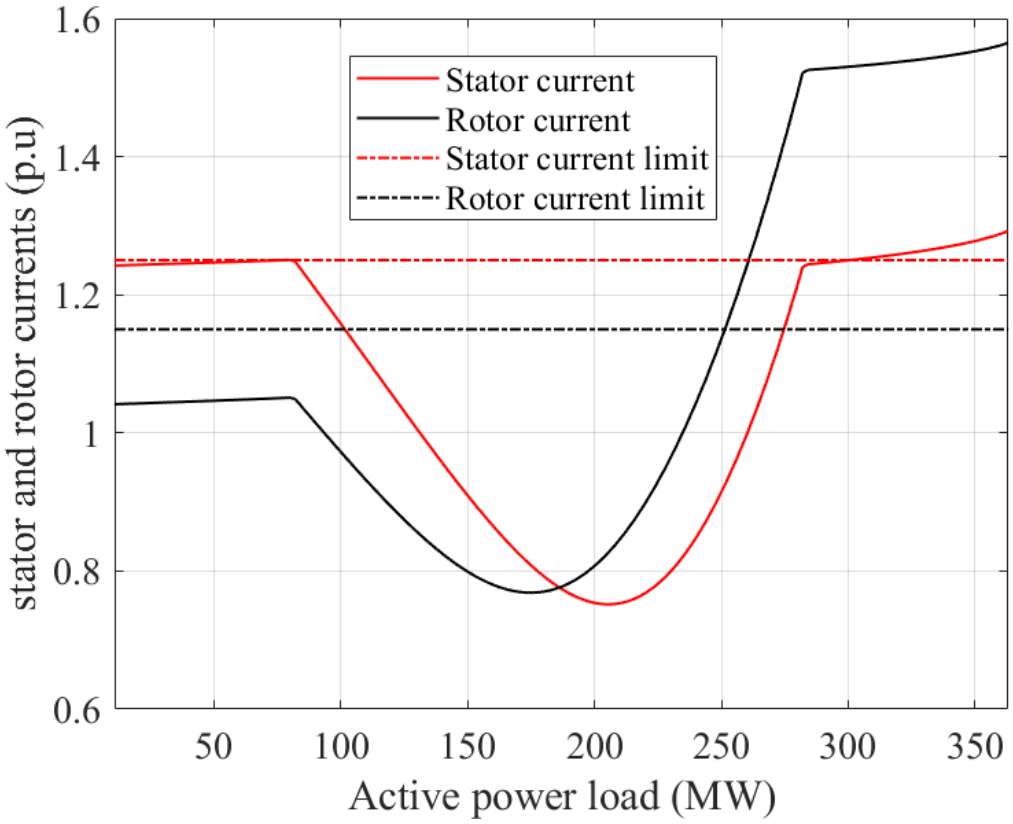

Figure 4.4: Stator and rotor currents for the system with fixed reactive power limits

It is observed from table 4.1 that the Hopf bifurcation point is shifted when the system has variable reactive power limits. This shift in the point for different values of reference voltage at the PCC is due to the over/under estimation of the reactive power limits. The location of the load bus where the bifurcation analysis is performed also determines the shift in the bifurcation point when the system has variable reactive power limits based on the capability curve. This has to do with the proximity of the load buses to the PCC.

Table 4.1: Hopf bifurcation points of systems A and B

Load bus	Reference voltage	System A	System B
Bus 5	1 p.u	331 MW	317 MW
Bus 6	0.98 p.u	296 MW	304 MW
Bus 6	1 p.u	294 MW	316 MW
Bus 8	1 p.u	330 MW	326 MW

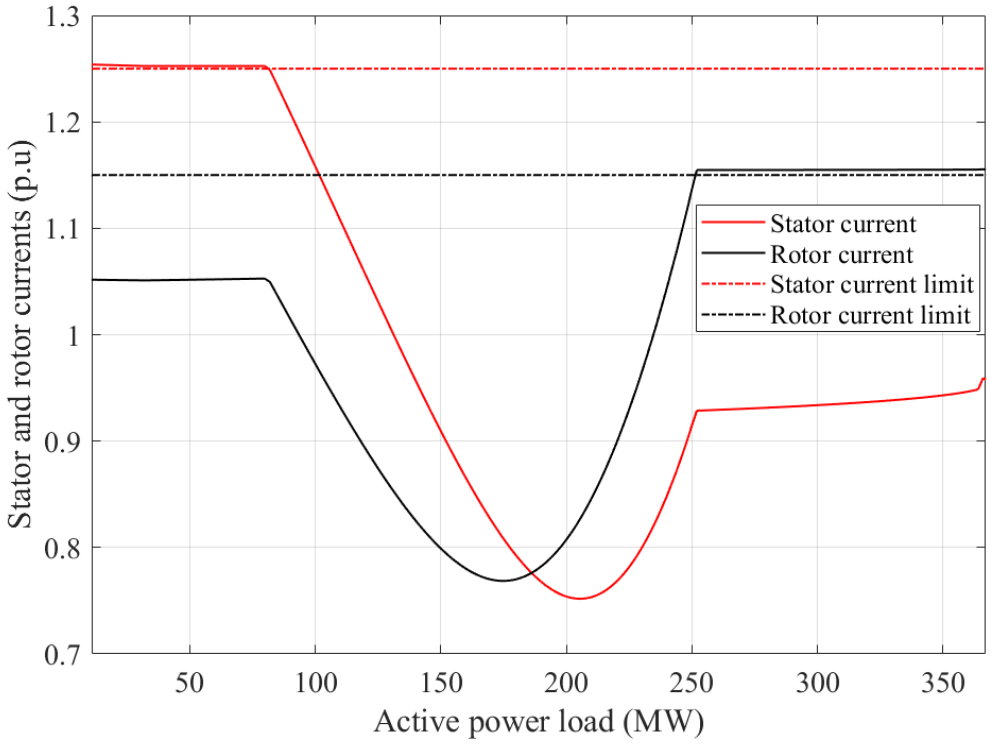

Figure 4.5: Stator and rotor currents for the system with variable reactive power limits

4.2.3 Results of time domain simulations

The system is subjected to a step change in the load at bus 5 and the results have been discussed in this section.

Response to a step change in the load

Figure 4.6 shows the evolution of stator and rotor currents of the DFIG when system A subjected to a step change in the load of 10% at time t = 0s. It is observed that the rotor current exceeds the maximum allowable limit. Figure 4.7 shows the variation of the stator and rotor currents of the DFIG in system A when the DFIG participates in frequency regulation through inertial control. When the step change in the load is encountered, the frequency of the system is supposed to drop. But with inertial response, the frequency nadir is reduced as the DFIG releases the stored energy in the rotor. When this happens, the rotor

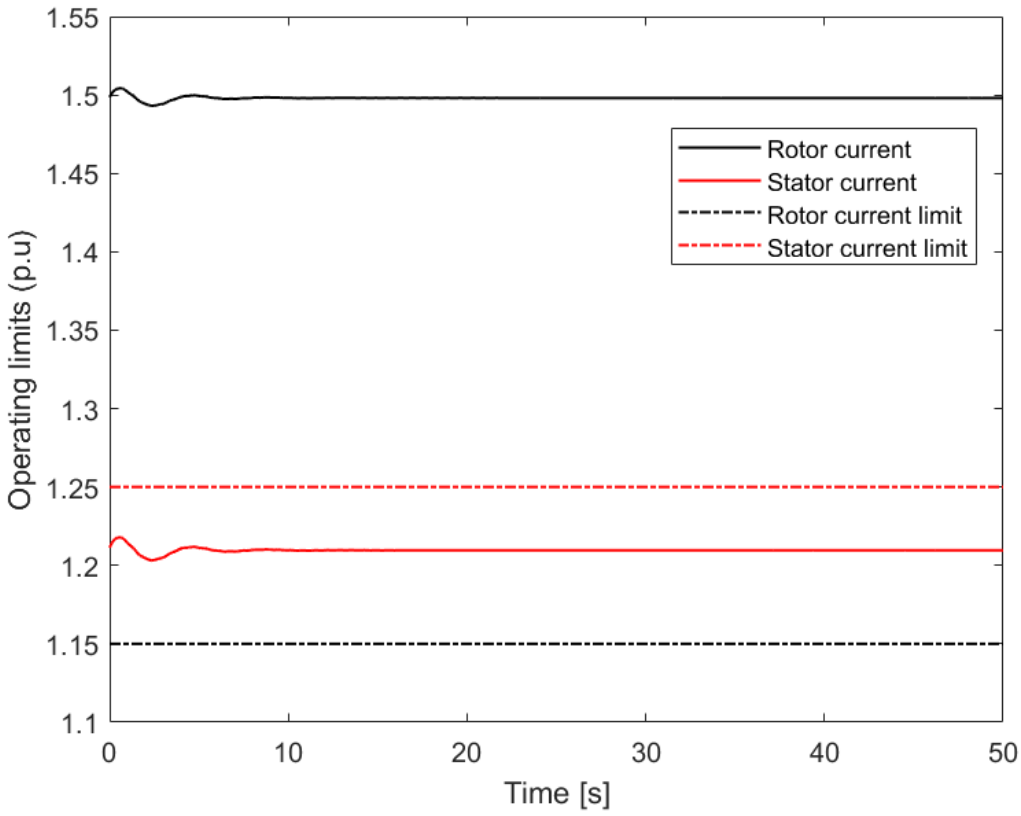

Figure 4.6: Variation of stator and rotor currents with time for a load step for system A

current increases. The rotor current is seen to exceed the maximum value when system A is subjected to the disturbance which in this case is the step change in the load.

Figures 4.8 and 4.9 show the variation of stator and rotor currents of the DFIG when system B is subjected to a step change in the load at bus 5. In this case, the stator and rotor currents are within the limits. The rotor current is at the maximum limit as the load in the system before the disturbance is at a level such that the system operates close to the rotor current limit. When the DFIG participates in frequency regulation by providing inertial response, the rotor current is at the limit and the stator current is within the maximum allowable limit.

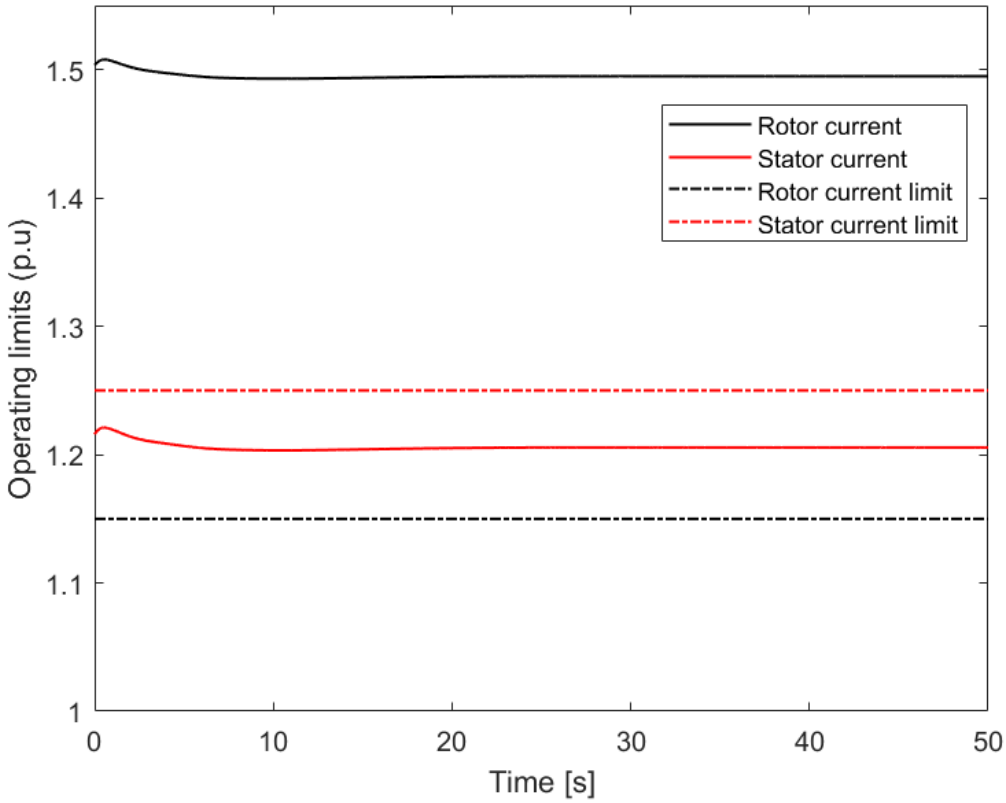

Figure 4.7: Variation of stator and rotor currents with time for a load step for system A with inertial control

Response to a change in the wind speed

The wind speed is assumed to be at 11 m/s before the occurrence of the disturbance. A change in the wind speed to 12 m/s is applied and the evolution of stator and rotor currents with respect to time are studied.

Figure 4.10 shows the variation of stator and rotor currents with time when the change in the wind speed is encountered in system A. The stator and rotor currents are found to exceed the maximum allowable limits with the occurrence of this disturbance.

The stator and rotor currents are plotted with respect to time when a change in the wind speed is encountered in system B as shown in figure 4.10. It can be observed that the stator and rotor currents are at the limit but do not exceed to high values above the maximum limits.

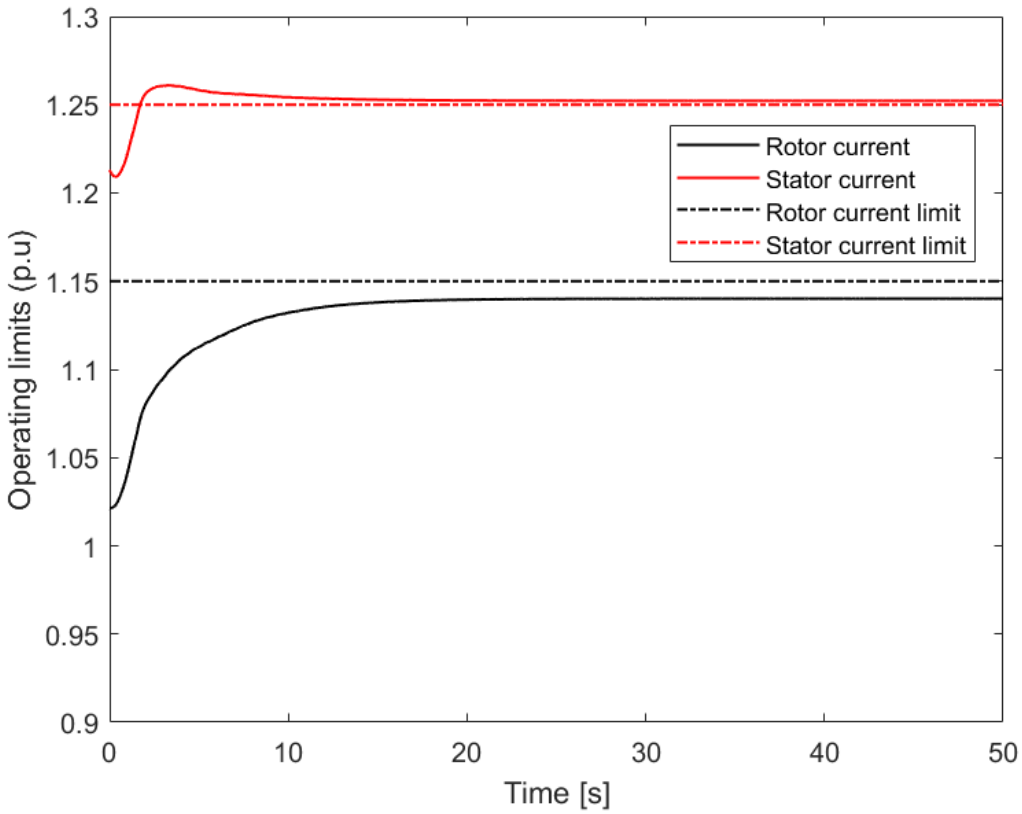

Figure 4.8: Variation of stator and rotor currents with time for a load step for system B

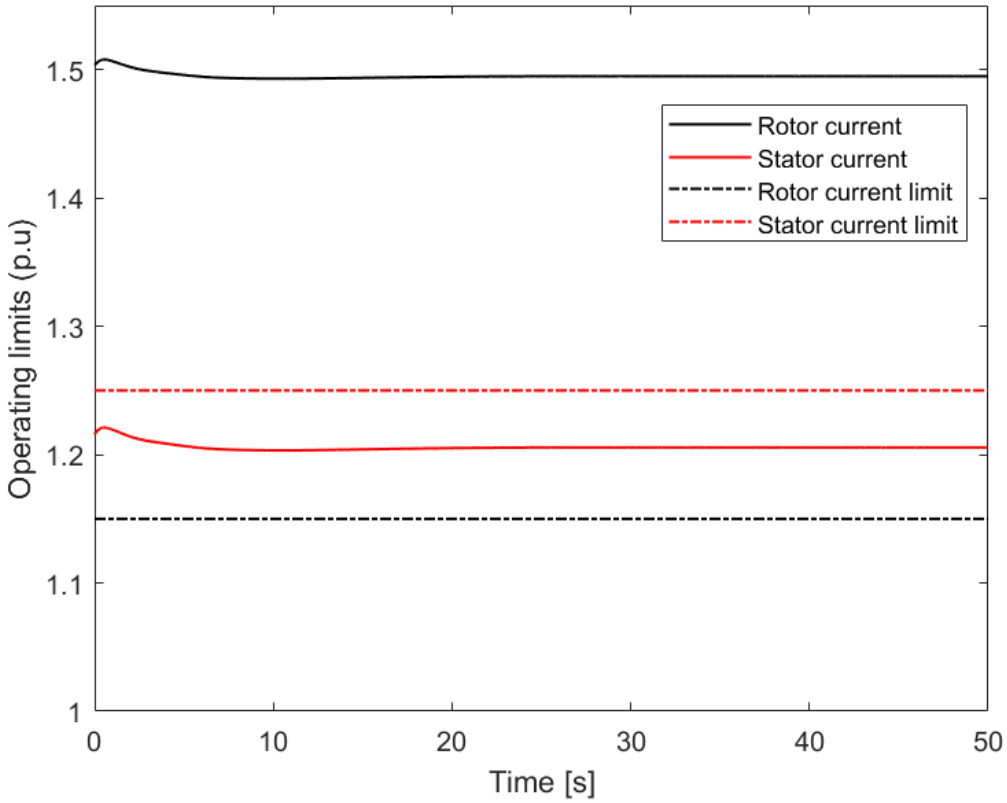

Figure 4.9: Variation of stator and rotor currents with time for a load step for system B with inertial control

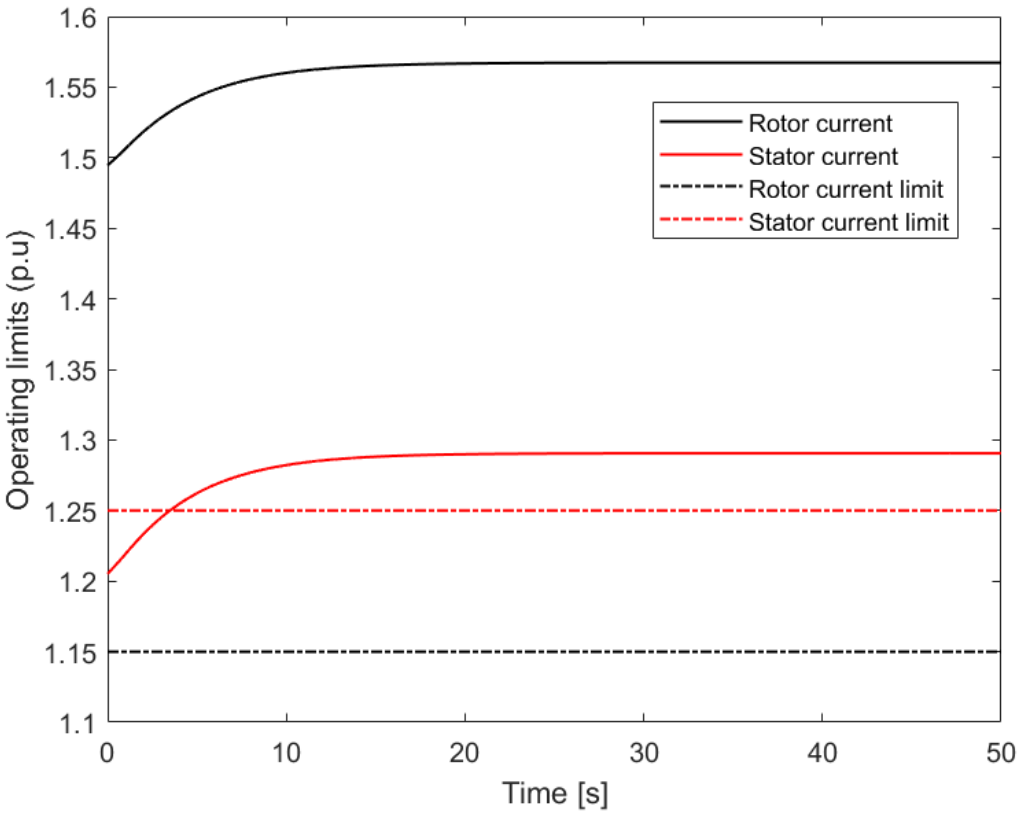

Figure 4.10: Variation of stator and rotor currents with time for a change in the wind speed for system A

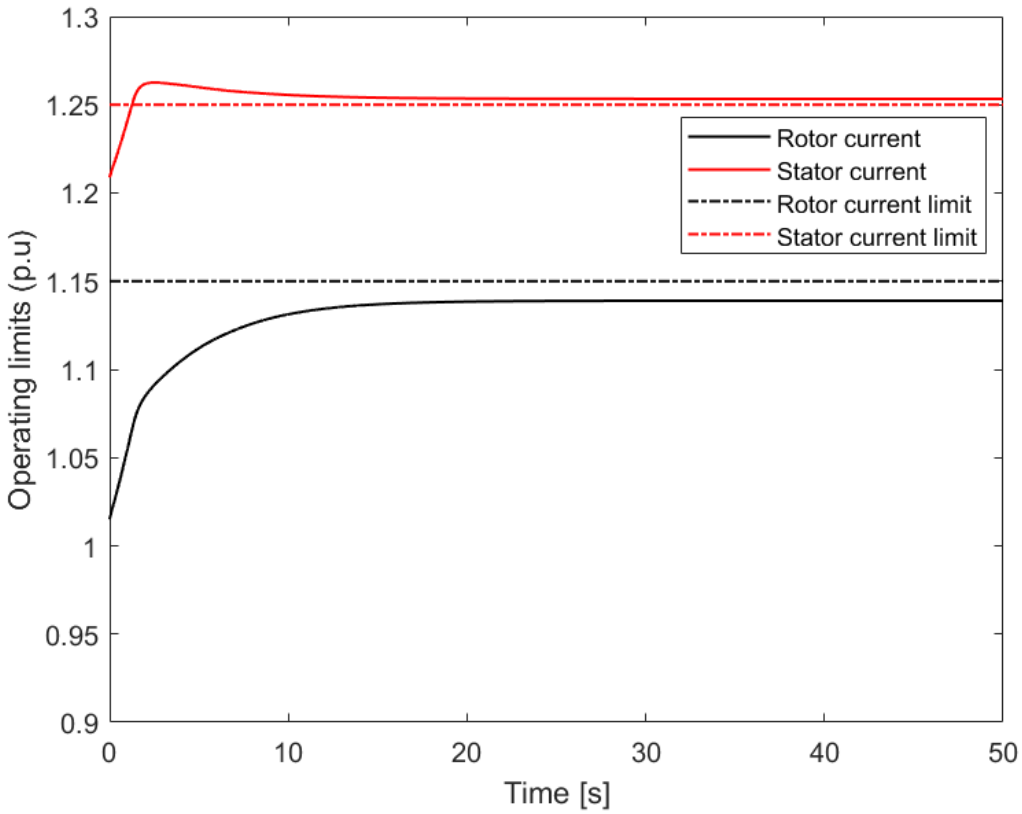

Figure 4.11: Variation of stator and rotor currents with time for a change in the wind speed for system B

Chapter 5

Conclusions

The reactive power limits based on the capability curve were implemented in the test system and the results of the bifurcation analysis considering the load as the bifurcation parameter as well as the results of the time domain simulation when the system was subjected to a step change in the load and a change in the wind speed were described in chapter 4. The conclusions which were drawn from this study have been summarized in this chapter.

5.1 Inference drawn from the study

1. The reactive power equations based on the capability curve have been derived assuming that the real power losses in the stator and rotor circuits are negligible as the resistances are very small compared to the reactances. The reactive power limit equation obtained was a quadratic equation which was solved to obtain the maximum and minimum values of reactive power available for a given value of real power generated by the DFIG and its operating slip.

2. The range of the active power load in which the voltage at the PCC could be regulated at the reference value was significantly different in the system with the reactive power limits based on the capability curves compared to the system with fixed reactive power limits in the DFIG because of the over/under estimation of the fixed reactive power

limits in the DFIG. Hence, with the application of the reactive power limits defined in this thesis, the possibility of over/under estimation of reactive power limits is avoided.

3. The rotor and stator current magnitudes were found to exceed the maximum limit allowable in the system with fixed reactive power limits in the DFIG whereas they were found to be at the maximum limit when the lower/upper limit of the supervisory control was binding. This was due to the fact that, at the lower limit of the supervisory control, the stator current limit dominates and at the upper level of supervisory control, the rotor current plays a limiting role.

4. In the time domain simulations, it was observed that the rotor and stator current magnitudes were well above the maximum limits for the system with fixed reactive power limits whereas the values were at the maximum limit or very close to it in the system with variable reactive power limits in the DFIG.

5. A more realistic method of estimating the reactive power limits has been presented in this thesis based on the capability curves. This would be a very useful tool for planning engineers for the wind farms as the problem of over/under estimating the reactive power capability is avoided using this method.

5.2 Future work

The reactive power limits including the real power losses in the circuit can be derived by representing the capability curves based on the stator and rotor currents which indirectly depend on the operating slip of the machine. This reduces the dimension of the equation by one. The coordination between wind farms at multiple locations in the power system for providing voltage regulation can be studied. The implementation of FACTS devices in order to support voltage regulation in the power system and the coordination between the FACTS devices and the DFIG based wind farms to support the voltage can also be studied.

Bibliography

[1] G. E. Likens, C. T. Driscoll, and D. C. Buso, "Long-term effects of acid rain: response and recovery of a forest ecosystem," *Science*, vol. 272, no. 5259, p. 244, 1996. 1

[2] S. H. Schneider, "The greenhouse effect- science and policy," *Science*, vol. 243, no. 4892, pp. 771–781, 1989. 1

[3] M. Hoel and S. Kverndokk, "Depletion of fossil fuels and the impacts of global warming," *Resource and energy economics*, vol. 18, no. 2, pp. 115–136, 1996. 1

[4] I. Dincer, "Renewable energy and sustainable development: a crucial review," *Renewable and Sustainable Energy Reviews*, vol. 4, no. 2, pp. 157–175, 2000. 1

[5] The European Wind Energy Association , *"Wind in Power, 2014 European Statistics",[Online].* Available at: http://www.ewea.org (Accessed in January 2016). 1

[6] S. N. Bhadra, D. Kastha, and S. Banerjee, *Wind electrical systems*. Oxford University Press, 2005. 1

[7] E. Camm, M. Behnke, O. Bolado, M. Bollen, M. Bradt, C. Brooks, W. Dilling, M. Edds, W. Hejdak, D. Houseman, *et al.*, "Characteristics of wind turbine generators for wind power plants," in *Power & Energy Society General Meeting, 2009. PES'09. IEEE*, pp. 1–5, IEEE, 2009. 1

[8] T. Ackermann, *Wind power in power systems*. John Wiley & Sons, 2005. 1

[9] M. Altin, Ö. Göksu, R. Teodorescu, P. Rodriguez, B.-B. Jensen, and L. Helle, "Overview of recent grid codes for wind power integration," in *Optimization of Electrical and Electronic Equipment (OPTIM), 2010 12th International Conference on*, pp. 1152–1160, IEEE, 2010. 2, 4

[10] M. Mohseni and S. M. Islam, "Review of international grid codes for wind power integration: Diversity, technology and a case for global standard," *Renewable and Sustainable Energy Reviews*, vol. 16, no. 6, pp. 3876–3890, 2012. 2

[11] H. A. Pulgar-Painemal and R. I. Glvez-Cubillos, "Limit-induced bifurcation by wind farm voltage supervisory control," *Electric Power Systems Research*, vol. 103, pp. 122 – 128, 2013. 2, 6, 9, 22

[12] M. Kayikci and J. V. Milanovic, "Reactive power control strategies for dfig-based plants," *IEEE Transactions on Energy Conversion*, vol. 22, no. 2, pp. 389–396, 2007. 3

[13] E. Vittal, M. O'Malley, and A. Keane, "Rotor angle stability with high penetrations of wind generation," *IEEE Transactions on Power Systems*, vol. 27, no. 1, pp. 353–362, 2012. 3

[14] A. Tapia, G. Tapia, and J. Ostolaza, "Reactive power control of wind farms for voltage control applications," *Renewable energy*, vol. 29, no. 3, pp. 377–392, 2004. 3

[15] F. M. Hughes, O. Anaya-Lara, N. Jenkins, and G. Strbac, "Control of dfig-based wind generation for power network support," *IEEE Transactions on Power Systems*, vol. 20, no. 4, pp. 1958–1966, 2005. 3

[16] R. J. Konopinski, P. Vijayan, and V. Ajjarapu, "Extended reactive capability of dfig wind parks for enhanced system performance," *IEEE Transactions on Power Systems*, vol. 24, no. 3, pp. 1346–1355, 2009. 3

[17] T. Lund, P. Sørensen, and J. Eek, "Reactive power capability of a wind turbine with doubly fed induction generator," *Wind energy*, vol. 10, no. 4, pp. 379–394, 2007. 4

[18] S. Engelhardt, I. Erlich, C. Feltes, J. Kretschmann, and F. Shewarega, "Reactive power capability of wind turbines based on doubly fed induction generators," *IEEE Transactions on Energy Conversion*, vol. 26, no. 1, pp. 364–372, 2011. 4

[19] H. A. Pulgar-Painemal and P. W. Sauer, "Doubly-fed induction machine in wind power generation," in *Electrical Manufacturing and Coil Winding Exposition*, 2009. 4

[20] W. Qiao and R. G. Harley, "Grid connection requirements and solutions for dfig wind turbines," in *Energy 2030 Conference, 2008. ENERGY 2008. IEEE*, pp. 1–8, IEEE, 2008. 4

[21] P. Krause, O. Wasynczuk, S. D. Sudhoff, and S. Pekarek, *Analysis of electric machinery and drive systems*, vol. 75. John Wiley & Sons, 2013. 4

[22] K. Clark, N. W. Miller, and J. J. Sanchez-Gasca, "Modeling of ge wind turbine-generators for grid studies," *GE Energy*, vol. 4, 2010. 4

[23] J. G. Slootweg, H. Polinder, and W. L. Kling, "Dynamic modelling of a wind turbine with doubly fed induction generator," in *Power Engineering Society Summer Meeting, 2001*, vol. 1, pp. 644–649 vol.1, July 2001. 4

[24] M. Kayikçi and J. V. Milanovic, "Dynamic contribution of dfig-based wind plants to system frequency disturbances," *IEEE Transactions on Power Systems*, vol. 24, no. 2, pp. 859–867, 2009. 4

[25] J. Morren, J. Pierik, and S. W. De Haan, "Inertial response of variable speed wind turbines," *Electric power systems research*, vol. 76, no. 11, pp. 980–987, 2006. 4

[26] V. Ajjarapu and B. Lee, "Bifurcation theory and its application to nonlinear dynamical phenomena in an electrical power system," *IEEE Transactions on Power Systems*, vol. 7, no. 1, pp. 424–431, 1992. 5

[27] H. A. Pulgar-Painemal and P. W. Sauer, "Bifurcations and loadability issues in power systems," in *PowerTech, 2009 IEEE Bucharest*, pp. 1–6, IEEE, 2009. 5

[28] K. Srivastava and S. Srivastava, "Elimination of dynamic bifurcation and chaos in power systems using facts devices," *IEEE Transactions on Circuits and Systems I: Fundamental Theory and Applications*, vol. 45, no. 1, pp. 72–78, 1998. 5

[29] N. Mithulananthan, C. A. Canizares, J. Reeve, and G. J. Rogers, "Comparison of pss, svc, and statcom controllers for damping power system oscillations," *IEEE transactions on power systems*, vol. 18, no. 2, pp. 786–792, 2003. 5

[30] H. A. Pulgar-Painemal and P. W. Sauer, "Dynamic modeling of wind power generation," in *North American Power Symposium (NAPS), 2009*, pp. 1–6, Oct 2009. 6

[31] H. Pulgar-Painemal and R. Galvez-Cubillos, "Wind farms participation in frequency regulation and its impact on power system damping," in *PowerTech (POWERTECH), 2013 IEEE Grenoble*, pp. 1–4, IEEE, 2013. 8, 10

[32] P. W. Sauer and M. Pai, "Power system dynamics and stability," *Urbana*, 1998. 22

Appendices

A Derivation of reactive power limits based on rotor current limit

$$G = \begin{bmatrix} g_{a1} + jb_{a1} & g_{a2} + jb_{a2} \\ g_{a3} + jb_{a3} & g_{a4} + jb_{a4} \end{bmatrix} \tag{1}$$

The real and reactive powers that can be produced for a given rotor current limit can be expressed based on the elements of the matrix in equation 1 as follows. Stator voltage is given by equation 3.8. The rotor current is expressed as $\bar{I}_{ar} = I_r e^{-j\theta}$.

$$P_s = {V_s}^2 g_{a1} + V_s I_r (g_{a2} \cos\theta + g_{b2} \sin\theta) \tag{2}$$

$$Q_s = -{V_s}^2 g_{b1} + V_s I_r (g_{a2} \sin\theta - g_{b2} \cos\theta) \tag{3}$$

Similarly, the real and reactive powers consumed by the rotor circuit can be expressed as follows.

$$P_r = s V_s I_r (g_{a3} \cos\theta - g_{b3} \sin\theta) + s g_{a4} {I_r}^2 \tag{4}$$

$$Q_r = s V_s I_r (g_{a3} \sin\theta + g_{b3} \cos\theta) + s g_{b4} {I_r}^2 \tag{5}$$

The net real power generated is expressed as $P_G = P_s - P_r$. Equation for P_G can be written as

$$P_G = k_2 + A_2 \cos\theta + B_2 \sin\theta \tag{6}$$

where

$k_2 = {V_s}^2 g_{a1} - s g_{a4} {I_r}^2$

$A_2 = V_s I_r (g_{a2} - s g_{a3})$

$B_2 = V_s I_r (g_{b2} + s g_{b3})$

Equation 6 is rewritten as

$$P_G - k_2 = R_2 \cos(\theta - \alpha) \tag{7}$$

where where

$R_2 = \sqrt{{A_2}^2 + {B_2}^2}$

$\tan\alpha = B_1/A_2$

Let

$$(P_G - k_2)/R_2 = \cos\gamma \tag{8}$$

Hence, equation 8 becomes

$$\cos(\theta - \alpha) = cos\gamma \tag{9}$$

The solution for θ from equation 9 is obtained as

$$\theta = \alpha \pm \gamma \tag{10}$$

Let

$$\begin{cases} \theta_1 = \alpha + \gamma \\ \theta_2 = \alpha - \gamma \end{cases} \tag{11}$$

The reactive power generated for a given rotor current limit is given by the same expression as in equation 3.

$$Q_G = -{V_s}^2 g_{b1} + V_s I_r (g_{a2} \sin\theta - g_{b2} \cos\theta) \tag{12}$$

When the values of θ_1 and θ_2 are substituted for θ in equation 12, the maximum and the minimum value of reactive power that can be produced for a given value of real power generated and operating slip can be obtained.

B Derivation of reactive power limits based on stator current limit

$$B = \begin{bmatrix} B_{a1} + jB_{b1} & B_{a2} + jB_{b2} \\ B_{a3} + jB_{b3} & B_{a4} + jB_{b4} \end{bmatrix} \tag{13}$$

The stator current is expressed as $\bar{I}_{as} = I_s e^{j\delta}$. The expressions for the real and reactive power generated for a particular stator current limit is given by the following equations.

$$P_s = V_s I_s \cos\delta \tag{14}$$

$$Q_s = V_s I_s \sin\delta \tag{15}$$

The expressions for real and reactive power absorbed by the rotor is given below.

$$\begin{aligned} P_r = {} & s(B_{a1}B_{a3} + B_{b1}B_{b3}){V_s}^2 + s(B_{a2}B_{a4} + B_{b2}B_{b4}){I_s}^2 \\ & + sV_sI_s(B_{a1}B_{a4} + B_{b1}B_{b4} + B_{a2}B_{a3} + B_{b2}B_{b3})\cos\delta \\ & + sV_sI_s(B_{a3}B_{b2} - B_{a2}B_{b3} + B_{a1}B_{b4} - B_{a4}B_{b1})\sin\delta \end{aligned} \tag{16}$$

$$\begin{aligned} Q_r = {} & s(B_{a3}B_{b1} - B_{a1}B_{b3}){V_s}^2 + s(B_{a4}B_{b2} - B_{a2}B_{b4}){I_s}^2 \\ & + sV_sI_s(B_{a4}B_{b1} - B_{a1}B_{b4} + B_{a3}B_{b2} - B_{a2}B_{b3})\cos\delta \\ & + sV_sI_s(B_{a1}B_{a4} + B_{b1}B_{b4} - B_{a2}B_{a3} - B_{b3}B_{b2})\sin\delta \end{aligned} \tag{17}$$

Net real power generated is given by $P_G = P_s - P_r$ which is obtained from expressions 14 and 16.

$$P_G = k_3 + A_3\cos\delta + B_3\sin\delta \tag{18}$$

where $k_3 = -s{V_s}^2(B_{a1}B_{a3} + B_{b1}B_{b3}) - s{I_s}^2(B_{a2}B_{a4} + B_{b2}B_{b4})$

$A_3 = V_sI_s[1 - s(B_{a1}B_{a4} + B_{b1}B_{b4} + B_{a2}B_{a3} + B_{b2}B_{b3})]$

$B_3 = -sV_sI_s[B_{a3}B_{b2} - B_{a2}B_{b3} - B_{a4}B_{b1} + B_{a1}B_{b4}]$

Equation 18 is rewritten as

$$P_G - k_3 = R_3 \cos(\delta - \alpha) \tag{19}$$

where

$R_3 = \sqrt{{A_3}^2 + {B_3}^2}$

$\tan\alpha = B_3/A_3$

Let $\frac{P_G - k_3}{R_3} = \gamma$. Then, equation 19 is rewritten as

$$\cos(\delta - \alpha) = \cos\gamma \tag{20}$$

Equation 20 is solved to obtain δ as

$$\delta = \alpha \pm \gamma \tag{21}$$

Let

$$\begin{cases} \delta_1 = \alpha + \gamma \\ \delta_2 = \alpha - \gamma \end{cases} \tag{22}$$

The reactive power generated is the same as that of equation 15 and can be rewritten as

$$Q_G = V_sI_s \sin\delta \tag{23}$$

Substituting the values of δ_1 and δ_2 for δ in equation 23, the maximum and the minimum values of reactive power that can be generated for a given slip and real power generation is obtained.

Vita

The author Jonathan Devadason has completed an undergraduate degree in electrical and electronics engineering in the year 2008 and a master's degree in power systems engineering in the year 2013 from College of Engineering, Anna University, India. He is currently working on his master's degree in electrical engineering in the University of Tennessee, Knoxville. His areas of interest are power system dynamics, application of power electronics in power systems - FACTS and HVDC transmission and bifurcations in power systems.